



AXISYMMETRIC MHD FLOW OF A VISCOUS FLUID IN A ROTATING CYLINDER

Dr. Harish Kumar

Associate Professor

Department of Mathematics

S.N.K.P. Govt. College, Neem Ka Thana- 332713 Rajasthan, India

ABSTRACT

We investigate the steady, ax symmetric, magneto hydrodynamic (MHD) flow of a viscous, Newtonian, incompressible, electrically-conducting fluid through an isotropic, homogeneous porous media situated in the annular zone between two concentric rotating cylinders in the presence of a radial magnetic field. The fluid in question is a viscous, Newtonian, incompressible, electrically-conducting fluid. The tangential and axial momentum equations, together with their related no-slip boundary conditions, are made non-dimensional by the use of transformation variables, which are also presented. By utilizing the Bessel and Lommel functions, one can arrive at solutions in closed-form. It was discovered that the axial velocity, denoted by UZ , drops by a significant amount as the Hartmann number, denoted by Ha , increases with the radial coordinate. Additionally, the profiles become progressively curved as the magnetic field becomes stronger. On display and under consideration here are illustrations and discussions of how the velocity is affected by newly discovered parameters such as third-grade parameters, second-grade parameters, and the Reynolds number. An equation for the skin-friction coefficient has been calculated and will now be provided. It was discovered that the thickness of the boundary layer for both velocity and momentum increased when the curvature parameter was increased. When compared to Newtonian and second-grade fluids with and without MHD effects for the instances (i) extending cylinder and (ii) flat plate, the velocity profile of third-grade fluid is greater than that of Newtonian and second-grade fluids.

Keywords: *Mhd, Cylinder, Fluid*

INTRODUCTION

In engineering science and applied mathematics, the study of hydro magnetic fluxes in rotating systems is predicted to remain a major area of focus. Analytical and numerical solutions to a wide range of geometric problems have been reported in a number of academic papers. These answers have been put forth. There are several uses that profit from the existence of such flows, including magneto hydrodynamic (MHD) energy producers, rocket propulsion control, crystal growth technologies, astrophysical plasma fluid dynamics, and tribological regulation in moving machine components. Transport in annular regimes, such as the annulus intercalated between rotating spheres or rotating cylinders, or even in rectangular annular ducts, has been the subject

of very little investigation. Flow in rotating annular areas is seen often in the oil and gas industry during the drilling process. An accurate simulation of the flow of the drilling mud in the annular area between the well wall and the drill pipe is necessary for evaluating the variability in the mud pressure within the well-bore, the frictional pressure drop, and the efficiency of the transport of the rock drill cuttings. It is also possible to utilize magnetic fields to control the outflow of fluid when that fluid is electrically conducting, sometimes known as ionized. The use of radial magnetic fields on concentric rotating cylinder systems can also provide fine tuning for the production of targeted chemicals. Modern computational fluid dynamics (CFD) techniques have greatly improved our ability to model hydromagnetic systems, but there is still a vast body of work to be done in terms of mathematical analysis. Such studies also serve as a solid reference point against which more complex simulations may be compared and CFD results can be validated. Someone in the late 1950s looked on fully formed laminar MHD flow in an annular channel, and their findings were crucial. This finding sparked a newfound fascination with hydromagnetic flow in revolving annuli. Wall suction and injection were studied for their potential impact on the Globe problem by both Jain and Mehta. Uberoi and Chow looked at the hydromagnetic viscous flow in a pipe annulus in more detail. When a radial magnetic field is applied to a system consisting of two concentric rotating cylinders, Nath found closed-form solutions for fully developed axial flow. These results showed that when the Hartmann number grew, both the axial and tangential velocity components decreased significantly. Hydromagnetic Newtonian flow in a rectangular annular channel was extensively studied by Baylis and Hunt. This builds on the work of Hunt and Stewartson, who proposed a similar concept in which conducting walls ran in the direction of the magnetic field and non-conducting walls ran perpendicular to it. examined the MHD flow between two concentric rotating cylinders in a uniform magnetic field, with a non-erodable and non-conducting porous lining on the inner wall of the outer cylinder, and discussed the effects of the ratio of the cylinder velocities, the slip parameter, the porosity parameter, and the Biot number on flow variables. Basu and Mandal solved the transient hydromagnetic flow between two co-axial cylinders using closed form finite Hankel transform solutions. These answers accounted for the influence of an induced magnetic field and showed that, as the magnetic field intensity grew, so did the frictional coupling per unit length. studied the presence of a radial magnetic field and its effect on the magnetohydrodynamic flow in an annular channel. In a computer study of the hydromagnetic stability of dissipative Couette flow in a rotating narrow gap annulus, it was shown that the presence of a magnetic field delays the onset of instability. The existence of conducting walls accentuates this effect more so than the presence of non-conducting walls. studied the magnetohydrodynamic circulation in the annulus generated by the rotation of eccentric cylinders. explored, computationally, the impact of wall mass flux on MHD viscoelastic flow in a cylinder-shaped annulus. Magnetohydrodynamic heat transport and flow in a liquid metal-gas annular regime under a transverse magnetic field was addressed by Li et al. (Li et al., 2005).

MATHEMATICAL MODEL

Let's have a look at the (r, z) -coordinated Newtonian steady incompressible electrically conducting viscous axial MHD flow between two insulating cylinders filled with an isotropic homogenous porous material that is completely saturated with the fluid. We shall pretend the

flow is incompressible and electrically conducting. According to Shercliff (Shercliff 1965), the effects of magnetic induction can be neglected if the magnetic Reynolds number is assumed to be small. The weak radial magnetic field imposed from outside can also mean that Hall current and ionslip current effects can be ignored. The electrical field dissipates everywhere and E is equal to zero when there is no charge separation and the body surface is not charged. Taylor vortices cannot form until an axial pressure gradient is applied, and the cylinders' rotational speeds are lower than the critical value. Taylor vortices are the desired result of this particular set of conditions. Figure 1 below illustrates the workout plan that will be followed.

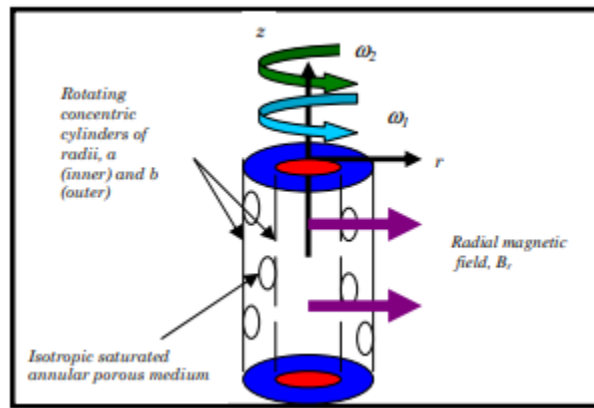


Figure 1: Both the Coordinate System and the Physical Model

Regardless of whether or not fully developed flow has been attained, Nath (Nath 1970) showed that the tangential velocity profile generated in a viscous liquid by rotating cylinders (in the absence of Taylor vortex motions) transforms into a function of the axial coordinate when an axial velocity is superimposed. An annulus is getting close to the completely formed condition when its tangential profile stops being reliant on its axial position. Constant electric current flowing perpendicular to the axis of the coaxial cylinders generates a radial magnetic field (B_r). In order to generate the radial magnetic field, the cylinders must terminate in perfect electrodes that are coupled to a load. Nath (Nath 1970) suggests that a permeability core inside the annulus and a permeable cylinder shell outside the annulus can also be used to achieve the goal of providing the required magnetic field. There are two permeable parts in this arrangement. Therefore, magnetic flux lines, if they took these porous paths, would always converge on a point far from the regime of interest.

Between the paths and the annulus channel are discs of permanently magnetized material that would act as the "source" of the magnetic flux. Nath (Nath 1970) and the Darcy drag force model illustrate how to simplify the Navier-Stokes equations in cylindrical coordinates for the magnetohydrodynamic saturated porous regime to the following form. Nath (1970) and Bég et al. (2009a, 2009b) provide evidence for this claim.

$$\frac{\rho u_{\theta}^2}{r} = \frac{\partial p}{\partial r} \quad (1)$$

$$u_{\theta} \frac{\partial u_{\theta}}{\partial z} = \nu \left[\frac{\partial^2 u_{\theta}}{\partial r^2} + \frac{1}{r} \frac{\partial u_{\theta}}{\partial r} - \frac{u_{\theta}^2}{r^2} + \frac{\partial^2 u_{\theta}}{\partial z^2} \right] - \frac{\sigma u_{\theta} B_r^2}{\rho} - \frac{\nu u_{\theta}}{K} \quad (2)$$

$$\frac{1}{\rho} \frac{\partial p}{\partial z} = \nu \left[\frac{\partial^2 u_z}{\partial r^2} + \frac{1}{r} \frac{\partial u_z}{\partial r} \right] - \frac{\sigma u_z B_r^2}{\rho} - \frac{\nu u_z}{K} \quad (3)$$

$$\frac{\partial}{\partial r}(rB_r) = 0 \quad (4)$$

where p is hydrostatic pressure, ρ is fluid density, σ is fluid electrical conductivity, ν is fluid kinematic viscosity, and K is porous medium permeability (isotropic hydraulic conductivity, meaning it is the same in both the r and z directions). Nath's study (Nath 1970) provided the basis for Equation (4), which implies that the radial

component of the magnetic field, B_r , is proportional to $\frac{1}{r}$. When the radius of the inner cylinder is a , we may infer that $B_r = A/a$ because $B_r = A/r$ in this case. To find solutions that are independent of the dimensions of the regime, we introduce the following non-dimensional variables:

$$P = \left(\frac{p}{0.5\rho\omega_2^2 b^2} \right), U_\theta = \frac{u_\theta}{\omega_2 b}, U_z = \frac{u_z}{\omega_2 b}, R = \frac{r}{b},$$

$$Z = \frac{z}{b}, \beta = \frac{B_r}{B_0} = \frac{1}{R}, Ha^2 = \frac{\sigma B_0^2 b^2}{\mu}, Re = \frac{\omega_2 b^2}{\nu},$$

$$Re \frac{\partial P}{\partial Z} = -\alpha \quad (\alpha > 0), \lambda = \frac{a}{b}, Da = \frac{K}{b^2} \quad (5)$$

in where P denotes the dimensionless pressure, U denotes the dimensionless tangential velocity, U_z denotes the dimensionless axial velocity, R denotes the dimensionless radial coordinate, Z denotes the dimensionless axial coordinate, β denotes the magnetic field ratio, B_0 denotes the typical magnetic induction, and Ha denotes the axial coordinate of the dimensionless pressure.

$\frac{\partial P}{\partial Z}$ represents the Hartmann number, The rotating Reynolds number is denoted by "Re.", $\frac{\partial P}{\partial Z}$ is the dimensionless axial pressure gradient, λ is the ratio of the cylinder's outer to its inner radius, and Da is the Darcy number. The following dimensionless equations are derived by adding variable (5) to equations (1) through (4):

$$\frac{\partial P}{\partial R} = \frac{1}{2} \frac{U_\theta^2}{R} \quad (6)$$

$$Re U_z \frac{\partial U_\theta}{\partial Z} - \frac{\partial^2 U_\theta}{\partial Z^2} = \frac{\partial^2 U_\theta}{\partial R^2} + \frac{1}{R} \frac{\partial U_\theta}{\partial R} - (1 + Ha^2) \frac{U_\theta}{R^2} - \frac{U_\theta}{Da} \quad (7)$$

$$\frac{\partial^2 U_z}{\partial R^2} + \frac{1}{R} \frac{\partial U_z}{\partial R} - \frac{Ha^2}{R^2} U_z - \frac{U_z}{Da} = -\alpha \quad (8)$$

The stated boundary conditions that are acceptable include the following:

$$U_\theta(R, 0) = 0; U_\theta(1, Z) = 1; \quad (9a)$$

$$U_\theta(\lambda, Z) = \frac{\omega_1 a}{\omega_2 b} = N; U_\theta(R, \infty) = 1 \quad (9b)$$

$$U_Z(1) = 0; U_Z(\lambda) = 1 \quad (9c)$$

3. Solution procedure

Homotopy is the foundational idea in topology that gave rise to homotopy analysis. Two functions are said to be homotopic if they may be continually transformed into each other. Two continuous functions f_1 and f_2 from topological space X to topological space Y are homotopic if and only if F is a continuous map and f_1 is homotopic to f_2 .

$$\text{Re}_z^{1/2} C_f = [f''(0) + 3\alpha_1 f''(0) + 2\beta \text{Re} f''(0)], \quad (10)$$

$$F: X \times [0, 1] \rightarrow Y \quad (11)$$

such that for each $x \in X$

$$F(x, 0) = f_1(x), \quad F(x, 1) = f_2(x) \quad (12)$$

If this is the case, then we say that map F is homotopic between functions f_1 and f_2 . In 1992, Liao proposed a method of homotopy analysis that might be used to solve the very nonlinear equations. This method is independent of any size- or scale-related physical properties. Homotopy is a continuous transformation that may be applied to a function or equation. Compared to other methods, it offers a number of advantages. First, it doesn't matter how large or tiny the input parameters are; second, it guarantees that the series solution will converge; and third, it gives you a lot of leeway in choosing the base function and the linear operator. This flexibility and freedom has been invaluable as we work to address some very complex problems. The linear operator used in the homotopy analysis method is taken from the linear part of the differential equation, as should be noted. However, to ease rapid study of convergence in a semi-infinite domain, it is advised to do it in a way that the solution appears as exponential functions. Homotopy analysis necessitates a guess for f_0 and g and a linear operator L_f in the following forms:

$$f_0(\eta) = 1 - \exp(-\eta), \quad (13)$$

$$\mathcal{L}_f(f(\eta)) = \frac{d^3 f}{d\eta^3} - \frac{df}{d\eta}, \quad (14)$$

whose characteristics include those listed below:

$$\mathcal{L}_f(C_1 + C_2 \exp(\eta) + C_3 \exp(-\eta)) = 0, \quad (15)$$

where $C_i \in \mathbb{R}, i = 1, 2, 3$ are the constants.

Zeroth-order deformation problem

The zeroth-order deformation equation is

$$(1 - q) [\hat{f}(\eta, q) - f_0(\eta)] = q H_j h_j \mathcal{N}[\hat{f}(\eta, q)], \quad (16)$$

Assuming the auxiliary convergence function H_f is equal to 1, and in the case when the

$$\begin{aligned} \mathcal{N}[\hat{f}(\eta, q)] = & (1 + 2\gamma\eta) \frac{\partial^3 \hat{f}}{\partial \eta^3} + 2\gamma \frac{\partial^2 \hat{f}}{\partial \eta^2} - \left(\frac{\partial \hat{f}}{\partial \eta} \right)^2 + f \frac{\partial^2 \hat{f}}{\partial \eta^2} \\ & + \alpha_1 \left[(1 + 2\gamma\eta) \left\{ 2 \frac{\partial \hat{f}}{\partial \eta} \frac{\partial^3 \hat{f}}{\partial \eta^3} - f \frac{\partial^4 \hat{f}}{\partial \eta^4} + 3 \left(\frac{\partial^2 \hat{f}}{\partial \eta^2} \right)^2 \right\} \right] \\ & + \gamma \left(6 \frac{\partial \hat{f}}{\partial \eta} \frac{\partial^2 \hat{f}}{\partial \eta^2} - 2f \frac{\partial^3 \hat{f}}{\partial \eta^3} \right) \\ & + \alpha_2 \left[2(1 + 2\gamma\eta) \left(\frac{\partial^2 \hat{f}}{\partial \eta^2} \right)^2 + \gamma \left(2 \frac{\partial \hat{f}}{\partial \eta} \frac{\partial^2 \hat{f}}{\partial \eta^2} + 2f \frac{\partial^3 \hat{f}}{\partial \eta^3} \right) \right] \\ & + \beta \text{Re} \left[6(1 + 2\gamma\eta)^2 \left(\frac{\partial^2 \hat{f}}{\partial \eta^2} \right)^2 \frac{\partial^3 \hat{f}}{\partial \eta^3} + 8\gamma(1 + 2\gamma\eta) \left(\frac{\partial^2 \hat{f}}{\partial \eta^2} \right)^3 \right] - M^2 \frac{\partial^2 \hat{f}}{\partial \eta^2}. \end{aligned} \quad (17)$$

Convergence of the developed solution

An additional parameter, hf , is involved in the 23rd homotopy series solution. Managing and controlling the convergence of the series solution (23) is largely dependent on this parameter, as stated above. The h -curve is shown in Figure 2 at the 13th order of approximation, which yields an adequate range of hf . The ranges of 1:1 to 6 hf and 0:2 to 6 hf are demonstrated in Fig. 1. In addition, Table 1 displays the results of an analysis of the series solution's convergence. Using this table, we can demonstrate that the series solution converges up to the 12th order of approximation.

Results and discussion

We have offered a discussion of the influence that a variety of intriguing physical qualities have on the velocity field through the use of graphs. This talk was about how the velocity field is affected by the characteristics.

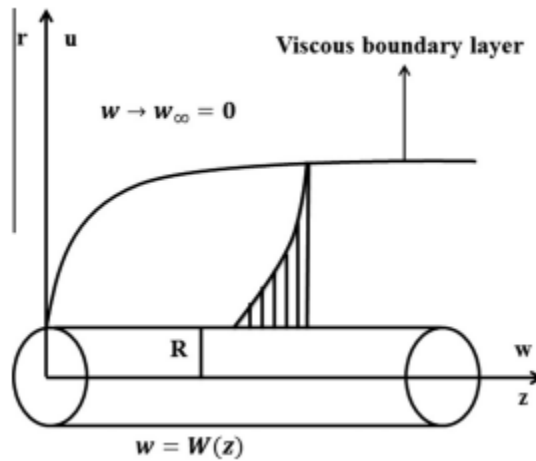


Figure 1 Physical flow model.

Table 1 Convergence of the homotopy solution occurs when the following values are true: $\alpha_1 = 0.1$, $\alpha_2 = 0.2$, $\beta = 0.05$, $\gamma = 0.2$, $M = 0.5$, and $Re = 0.5$.

Order of approximation	$f''(0)$
1	0.92348
2	0.93113
5	0.92826
10	0.92813
12	0.92812
24	0.92812
25	0.92812
30	0.92812

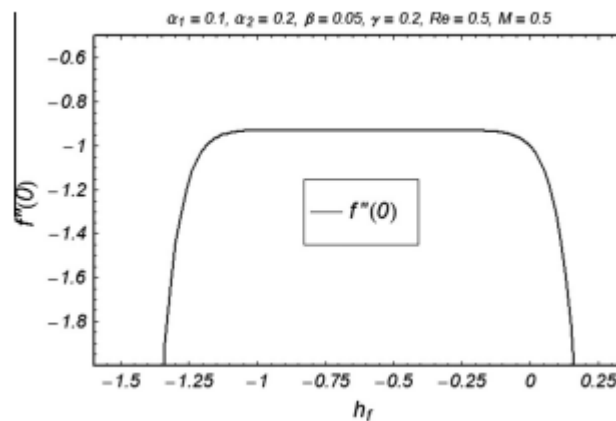


Figure 2 at the thirteenth order of approximation, the h curve for f.

Numerical values of the skin friction coefficient $Re^{1/2} z C_f$ are provided for convenience, and the effect of dimensionless variables on this quantity is analyzed.

Figure 3 depicts a possible change in the impact of the magnetic parameter M on the scalar velocity $f(0)$. It has been observed that the profile of velocities decreases with increasing M . In

addition, the momentum boundary layer thins out. Reduced velocities and momentum at the boundary are the result of the Lorentz force $M^2 f' 0 g$ that results from an external magnetic field. This is because the Lorentz force exerts a real, material, and tangible influence. The time-dependent variation of the shear thickening/thinning parameter is shown in Figure 4. The velocity and momentum boundary layer thickness is shown to decrease with increasing b . The figure below shows an example of this. So, it would appear that M and b behave similarly. Figure 5 displays, for a variety of values of a_1 , the variation of $f' 0 g$ with respect to g . This diagram shows how the thickness of the momentum boundary layer and the velocity profile both grow as a_1 increases. Similar results can be obtained for the variable a_2 in Fig. 6. Fig. 7 was made to investigate how the curvature parameter c influences the velocity distribution. Images like this one show that when c , the value of the curvature parameter, increases, the velocity $f' 0 g$ and the thickness of the momentum boundary layer both grow. A smaller radius for the cylinder results from increasing the curvature parameter c . The resistance to the flow of the fluid likewise lowers because the area of the cylinder in contact with the fluid shrinks. From a purely physical perspective, this is why we see this occurrence. The result is a steeper profile of increasing velocity. Figure 8 provides a more in-depth explanation of the influence of Reynolds number Re on the velocity profile $f(\eta)$ vs. g . Raising the Reynolds number, Re , has the following effect:

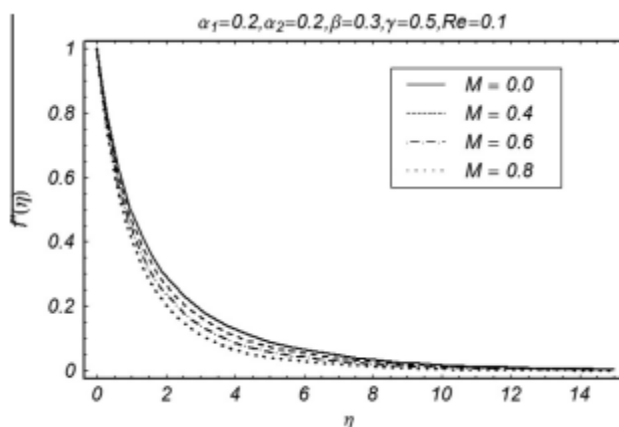


Figure 3 The following diagram illustrates the connection between the magnetic parameter M and the velocity component $f(\eta)$.

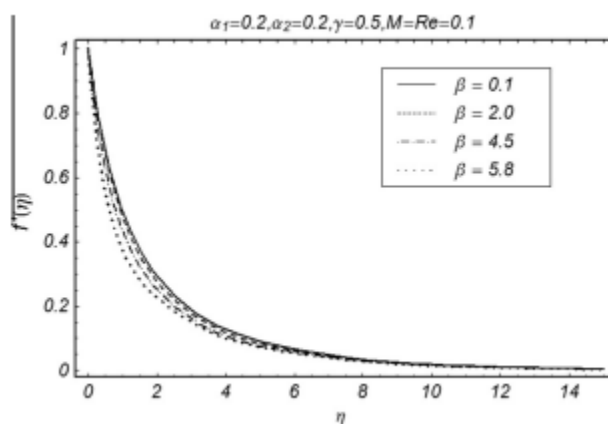


Figure 4 Below is a graph depicting the third-grade parameter b 's connection with the velocity component $f(\eta)$.

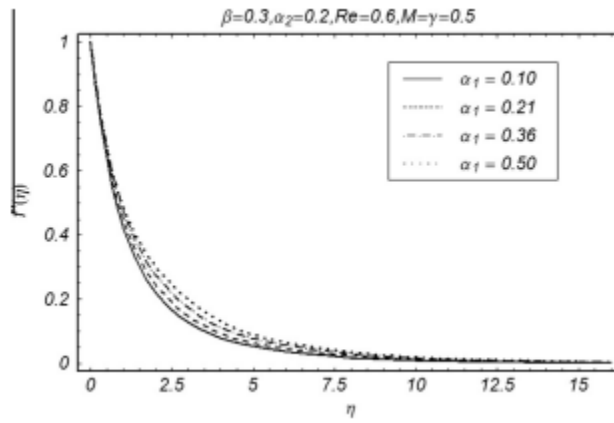


Figure 5 Relating the second-grade parameter α_1 to the velocity term $f(\eta)$ graphically.

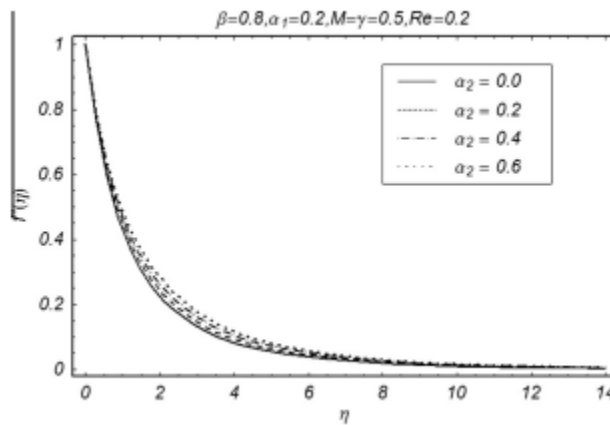


Figure 6 The following diagram illustrates the link that exists between the velocity component $f(\eta)$ and the value of g for the second-grade parameter a_2 .

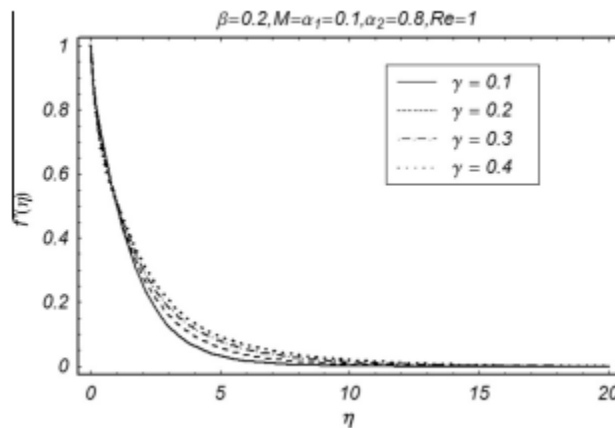


Figure 7 The diagram below illustrates the link that exists between the curvature parameter c and the velocity component $f(\eta)$.

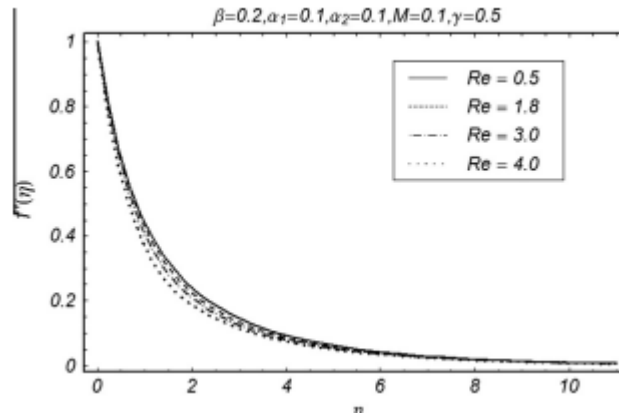


Figure 8 The relationship between the velocity component $f(\eta)$ and the Reynolds number Re is seen below.

because the profile's overall velocity has slowed down as a result. In addition to that, the thickness of the momentum barrier layer goes down as it moves away. In the presence of a magnetic parameter, the viscous, second-grade, and third-grade fluid velocities along a stretched cylinder are compared to one another in Fig. 9, which is a graphic that depicts the comparison. The findings of the research indicate that viscous fluid and second-grade fluid both have velocities that are much lower than those of third-grade fluid, which has a significantly higher velocity. The viscous fluid, on the other hand, flows at a significantly slower rate in comparison to the second-grade fluid, which has a higher velocity. A comparison between fluid at the third-grade level, fluid at the second-grade level, and viscous fluid

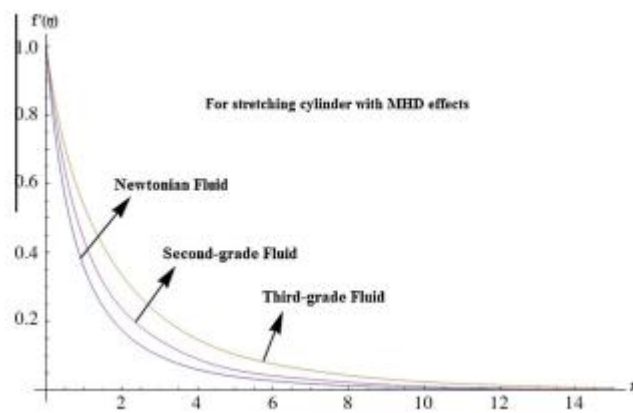


Figure 9 In the presence of magnetic effects and with c equal to 0.2, the velocity profile for viscous, second-grade, and third-grade fluids is shown below.

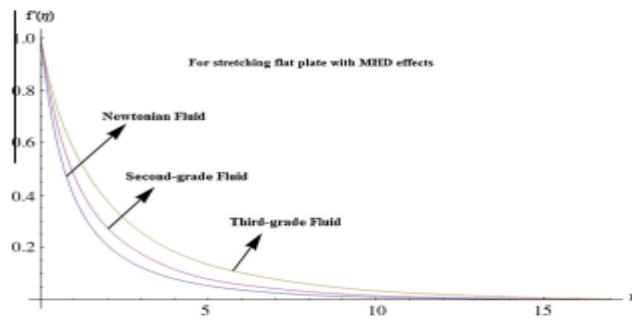


Figure 10 The velocity profile for viscous, second-grade, and third-grade fluids is illustrated below with the value of c equal to 0 when they are subjected to magnetic effects as described in the previous sentence.

Figure 10 illustrates the velocities together with the magnetic parameter M as they travel across a flat plate. However, the velocity of second-grade fluid is lower than that of third-grade fluid but higher than that of viscous fluid, whereas the velocity of third-grade fluid is lower than that of second-grade fluid but higher than that of viscous fluid. Viscous fluid has a velocity that is lower than that of second-grade fluid but higher than that of third-grade fluid.

Conclusion

In order to explore the hydromagnetic flow of third-grade fluid over a stretched cylinder, the homotopic approach is applied as a research technique. The following table presents the results of this inquiry, with an emphasis on the most significant discoveries. The shear thinning/thickening parameter b and the magnetic parameter M both need to be raised for the velocity profile to go in the other direction, which is downward. When the Reynolds number Re is increased, the radial velocity f_0 and the thickness of the momentum boundary layer are both functions that decrease. It may be said that the effects that the dimensionless parameters a_1 and a_2 have on the radial velocity f_0 are relatively comparable to one another in terms of their qualitative manifestations. When the values of the variables a_1 , b , Re , c , and M are all decreased, while the value of the variable a_2 is increased, it is demonstrated that the skin friction coefficient, $Re^{1/2} C_f$, has very small values. In both the flat plate and the cylinder, the third-grade fluid results in a higher increase in the velocity profile, regardless of whether or not the magnetic parameter is present. This is in contrast to the velocity profile for the viscous fluid and the second-grade fluid, which can be found below.

References

- [1] T. Chinyoka, O.D. Makinde, Unsteady hydromagnetic flow of a reactive variable viscosity third-grade fluid in a channel with convective cooling, *Int. J. Numer. Methods Fluids* 69 (2012) 353–365.
- [2] T. Hayat, R. Naz, S. Asghar, S. Mesloub, Soret–Dufour effects on three-dimensional flow of third grade fluid, *Nucl. Eng. Des.* 243 (2012) 1–14.
- [3] B. Sahoo, Y. Do, Effects of slip on sheet driven flow and heat transfer of a third grade fluid past a stretching sheet, *Int. Commun. Heat Mass Transfer* 37 (2010) 1064–1071.
- [4] S. Abbasbandy, T. Hayat, On series solution for unsteady boundary layer equations in a special third grade fluid, *Commun. Nonlinear Sci. Numer. Simul.* 16 (2011) 3140–3148.

- [5] T. Hayat, Z. Iqbal, M. Mustafa, A.A. Hendi, Melting heat transfer in the stagnation point flow of third-grade fluid past a stretching sheet with viscous dissipation, *Therm. Sci.* 17 (3) (2013) 865–875.
- [6] A. Shafiq, M. Nawaz, T. Hayat, A. Alsaedi, Magnetohydrodynamic axisymmetric flow of a third-grade fluid between two porous disks, *Br. J. Chem. Eng.* 30 (3) (2013) 599–609.
- [7] M. Hatami, J. Hatami, D.D. Ganji, Computer simulation of MHD blood conveying gold nanoparticles as a third grade nonNewtonian nanofluid in a hollow porous vessel, *Comput. Methods Program. Biomed.* (2013).
- [8] T. Hayat, S.A. Shehzad, M. Qasim, S. Asghar, A. Alsaedi, Thermally stratified radiative flow of third grade fluid over a stretching surface, *J. Thermophys. Heat Transfer* 28 (2014) 155–161.
- [9] C.Y. Wang, Fluid flow due to a stretching cylinder, *Phys. Fluids* 31 (1988) 466.
- [10] S. Mukhopadhyay, MHD boundary layer slip flow along a stretching cylinder, *Ain Shams Eng. J.* 4 (2012) 317–324.
- [11] H. Ashorynejad, M. Sheikholeslami, I. Pop, D. Ganji, Nanofluid flow and heat transfer due to a stretching cylinder in the presence of magnetic field, *Heat Mass Transfer* 49 (2013) 427–436.
- [12] C.Y. Wang, Natural convection on a vertical stretching cylinder, *Commun. Non-linear Sci. Numer. Simul.* 17 (2012) 1098–1103.
- [13] S. Nadeem, A. Rehman, C. Lee, J. Lee, *Boundary Layer Flow of Second-grade Fluid in a Cylinder with Heat Transfer*, Hindawi Publishing Corporation, 2012, p. 13.
- [14] S. Mukhopadhyay, R.S.R. Gorla, Slip effects on boundary layer flow and heat transfer along a stretching cylinder, *Ain Shams Eng. J.* 4 (2012) 317–324.
- [15] R.S.R. Gorla, A.J. Chamkha, E. Al-Meshaie, Melting heat transfer in a nanofluid boundary layer on a stretching circular cylinder, *J. Naval Arch. Marine Eng.* 9 (2012) 1–10.
- [16] A. Rehman, S. Nadeem, Mixed convection heat transfer in micropolar nanofluid over a vertical slender cylinder, *Chin. Phys. Lett.* 29 (2012) 124701.
- [17] N. Bachok, A. Ishak, Flow and heat transfer over a stretching cylinder with prescribed surface heat flux, *Malay. J. Math. Sci.* 4 (2) (2010) 159–169.